Mon. Not. R. Astron. Soc. **395,** 2045–2055 (2009) doi:10.1111/j.1365-2966.2008.14188.x

Multifrequency study of the ring nebula SG 13

J. Vasquez,[1,2]★† C. E. Cappa[1,2]‡ and S. Pineault[1,3]

[1]*Instituto Argentino de Radioastronomía (CCT-La Plata, CONICET), C.C.5., 1894 Villa Elisa, Argentina*
[2]*Facultad de Ciencias Astronómicas y Geofísicas, Universidad Nacional de La Plata, La Plata, Argentina*
[3]*Départment du physique, de génie physique et d'optique and Centre de recherche en astrophysique du Québec (CRAQ), Université Laval, Québec GIVOA6, Canada*

Accepted 2008 November 3. Received 2008 October 22; in original form 2008 September 18

ABSTRACT

We investigate the morphology and kinematics of the interstellar medium in the environs of the open cluster Mrk 50, which includes the Wolf–Rayet star WR 157 and a number of early B-type stars. The analysis was performed using radio continuum images at 408 and 1420 MHz, and H I 21-cm line data taken from the Canadian Galactic Plane Survey, molecular observations of the ^{12}CO ($J = 1 \rightarrow 0$) line at 115 GHz from the Five College Radio Astronomy Observatory and available mid- and far-infrared (FIR) observations obtained with the Midcourse Space Experiment and *IRAS* satellites, respectively.

This study allowed the identification of the radio continuum and molecular counterpart of the ring nebula SG 13, while no neutral atomic structure was found to be associated. The nebula is also detected in the images in the mid- and FIR, showing the existence of dust well mixed with the ionized gas. We estimate the main physical parameters of the material linked to the nebula.

The interstellar gas distribution in the environs of Mrk 50 is compatible with a stellar wind bubble created by the mass loss from WR 157.

The distribution of young stellar object candidates in the region shows that the stellar formation activity may be present in the molecular shell that encircles the ring nebula.

Key words: stars: Wolf–Rayet – ISM: bubbles – H II regions.

1 INTRODUCTION

Massive stars inject large amounts of energy into the interstellar medium (ISM) through stellar winds, through ultraviolet (UV) radiation and during their supernova (SN) phase at the end of their lives. Therefore, the morphology, dynamics and energetics of their interstellar environment are strongly modified by the presence of these stars.

Wolf–Rayet (WR) stars are commonly believed to be the evolved O-type stars which have almost reached the end of their nuclear burning phase (Conti 1976; Maeder 1983; van der Hucht 2001). They are characterized by an intense mass flow with the mass-loss rates of $\sim$(1–5) $\times$ 10^{-5} $M_{\odot}$ yr^{-1} (Cappa, Goss & Pineault 2004) and the terminal velocities of 1000–3000 km s^{-1} (van der Hucht 2001 and references therein) which sweeps up the surrounding interstellar matter. The gas shed by the star and the swept-up interstellar material are piled-up in expanding shells, called *interstellar bubbles* (IBs). Stellar wind shocks modify the temperature, presure and density of the surrounding ISM. The strong UV photon flux (with $h\nu \geq 13.6$ eV) of these stars ionizes the bubbles, which are detected in the optical and radio ranges as ring nebulae. When the ionization front is trapped in the expanding IBs, these structures have a neutral outer layer which can be detected in the H I 21-cm line emission. The emission distribution of this radio line in the environs of these stars has shown the presence of cavities and expanding shells linked to the stars and their optical IBs (e.g. Vasquez et al. 2005 and references therein). Molecular gas related to IBs has also been found in a number of cases (Cappa, Rubio & Goss 2001).

Stellar formation may be favoured in the cold and dense outer shells, following the mechanism proposed by Elmegreen & Lada (1977) and Elmegreen (2000). In their model, massive stars excite an H II region that expands and sweeps up a shell of shocked cold neutral gas. Eventually, the dense shell of cold neutral swept-up gas formed around these stars fragments and collapses to produce a new generation of stars. Up to now, very few studies dealing with the stellar formation in the molecular shells of IBs have been carried out (see e.g. Oey 1996), and this point is still an open question.

In this paper, we report the results of a multifrequency study of the gas distribution around WR 157 and its optical ring nebula based on both the IR and radio data. Stellar formation activity in the region and its relation to the stellar wind bubble are also investigated.

★Post-doctoral fellow of CONICET, Argentina.
†E-mail: jvasquez@fcaglp.unlp.edu.ar
‡Member of Carrera del Investigador, CONICET, Argentina.

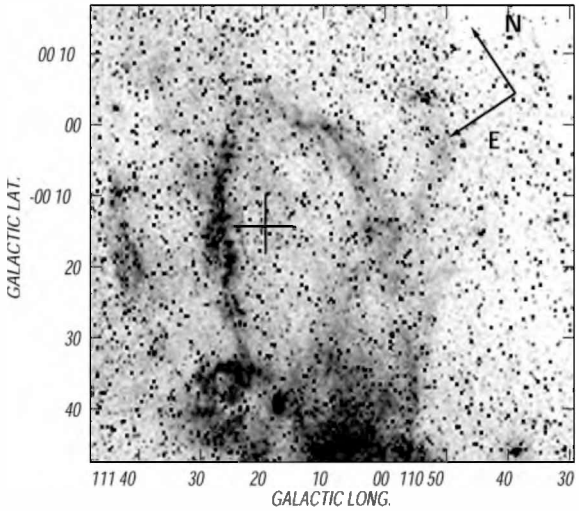

Figure 1. DSS *R* image of SG 13. The cross marks the location of WR 157. The grey-scale is in arbitrary units.

2 WR 157 AND ITS OPTICAL RING NEBULA

Sh2-157 (Sharpless 1959) consists of two different regions: SG 13 (=Simeiz 274) at $b > -0^{\circ}35'$ (Shain 1951) which has a claw-like appearance and SG 14, placed at $b < -0^{\circ}35'$, which is diffuse and irregular in shape. SG 13 is associated with the open cluster Markarian 50 (Mrk 50; Turner et al. 1983; Lündstron & Stenholm 1984; Smith & Willis 1994) located at $(l, b) = (111^{\circ}21', -0^{\circ}12')$, (RA, Dec. [J2000]) = ($23^{\rm h}12^{\rm m}$, $+60^{\circ}29'$). The brightest member of this cluster is the WR star WR 157 [=HD 219460, WN 5+B1II, $(l, b) = (111^{\circ}19\farcm8, -0^{\circ}13\farcm8)$, (RA, Dec. [J2000]) = ($23^{\rm h}15^{\rm m}12\fs40$, $+60^{\circ}27'01\farcs8$); van der Hucht 2001].

SG 13 and Mrk 50 are located in the Perseus spiral arm. Based on CCD $UBV(RI)_C$ photometry, Baume, Vazquez & Carraro (2004) derived a photometric distance $d_{\rm Mrk\,50} = 3.46 \pm 0.35$ kpc for the open cluster. van der Hucht (2001) gives a spectrophotometric distance $d = 3.4$ kpc for WR 157, based on its association with the cluster.

Fig. 1 displays the Digitized Sky Survey (DSS) *R* image of SG 13. The cross indicates the position of WR 157. The ring nebula around Mrk 50 is easily identified as a claw-like emission region of $\simeq 35 \times 40$ arcmin^2 in size, with the open cluster close to the brightest section of SG 13. The diffuse emission at Galactic latitudes $b \leq -0^{\circ}35'$ corresponds to SG 14.

From [O III] 5007 Å, [N II] 6584 Å and [S II] 6717+6731 Å observations, Lozinskaya et al. (1986) found that the local standard of rest (LSR) velocity of SG 13 is in the range -53 to -33 km s^{-1}. This result is consistent with the studies of bright regions in SG 14 based on the H166α radio recombination lines (RRL) (-43 km s^{-1}; Pedlar 1980), CO observations (Blitz, Fich & Stark 1982) and Hα data (Georgelin 1975).

The analytical fit to the Circular Galactic Rotation model by Brand & Blitz (1993) predicts that the velocities within the range -53 to -33 km s^{-1} are located at kinematical distances $d_{\rm k} \simeq 3.6$–5.7 kpc, compatible with the spectrophotometric distance to WR 157 and Mrk 50. A different kinematical distance was published by Georgelin, Georgelin & Roux (1973) and Georgelin & Georgelin (1976), who found $d = 2.5 \pm 0.4$ kpc. In what follows, we adopt a distance $d = 3.7 \pm 1.2$ kpc for SG 13.

3 OBSERVATIONS

The analysis of the gas distribution was performed using observations in the optical, IR and radio ranges. The DSS *R* image of Sh2-157 was obtained from the Skyview web page.[1]

3.1 Radio continuum, H I and CO data

To analyse the ionized and neutral atomic gas distribution, we used H I observations from the Canadian Galactic Plane Survey (CGPS) obtained with the synthesis telescope of the Dominion Radio Astrophysical Observatory (DRAO) in Canada. This telescope performed interferometric observations of the 21-cm H I spectral line, and, simultaneously, continuum emission in two bands centred at 1420 and 408 MHz. The east–west array consists of seven antennae, 9-m each. Single-dish data were routinely incorporated into the interferometric images to ensure complete coverage of the emission on all the angular scales down to the resolution limit. Radio continuum observations of the region of SG 13 have synthesized the beams of 3.4×3.9 arcmin^2 and 58×67 arcsec^2 at 408 and 1420 MHz, respectively. The measured rms image noises are 5 and 1.5 K at 408 and 1420 MHz, respectively. Details about DRAO and the CGPS can be found in Landecker et al. (2000) and Taylor et al. (2003).

To investigate the neutral hydrogen distribution, we extracted a data cube centred at $(l, b, v) = (111^{\circ}8', -0^{\circ}23', -40.2$ km s$^{-1})$ from the CGPS. The H I data have a synthesized beam of 1.13×0.98 arcmin^2, a rms noise of 3 K in bright temperature ($T_{\rm B}$) and a velocity resolution of 1.3 km s^{-1} with a channel separation of 0.824 km s^{-1}. The H I images were convolved to a 2×2 arcmin^2 beam size to facilitate the identification of structures. The observed velocities cover the range -60 to 163 km s^{-1}.

The ^{12}CO ($J = 1 \rightarrow 0$) line data at 115 GHz were obtained using the radio telescope of the Five College Radio Astronomy Observatory (FCRAO) in USA. The angular resolution is approximately 46 arcsec. Details about the CO survey are summarized by Ridge et al. (2006).

3.2 *IRAS* and MSX data

IR images at different wavelengths were used to analyse the dust distribution in the region. High-resolution IR images (HIRES), at 60 and 100 μm, were taken from the Infrared Processing and Analysis Center (IPAC)[2] with the angular resolutions of $\simeq$1 and 2 arcmin.

The Spatial IR Imaging Telescope (SPIRIT III) on board the Midcourse Space Experiment (MSX) satellite surveyed the entire Galactic plane in the four mid-IR bands centred at 8.28, 12.13, 14.65 and 21.3 μm (bands *A*, *C*, *D* and *E*, respectively). We retrieved images in the four bands with 18.4 arcsec in angular resolution from IPAC. We converted the flux densities to Janskys by using the conversion factor of radiance to flux density given in the MSX Image Server at IPAC (Egan et al. 1999).

To investigate the presence of pre-main-sequence stars towards the region under study, we extracted IR point sources from the MSX, 2MASS and *IRAS* point-source catalogues.

[1] http://skyview.gsfc.nasa.gov/

[2] IPAC is founded by NASA as part of the *IRAS* extended mission under contract to Jet Propulsion Laboratory (JPL) and California Institute of Technology (Caltech).

4 GAS AND DUST DISTRIBUTION

4.1 Radio continuum emission

The radio continuum images at 408 and 1420 MHz are shown in the top and middle panels of Fig. 2. The radio emission distribution at 1420 MHz correlates strikingly well with the optical emission (see the bottom panel of Fig. 2). The brightest optical emission region coincides with the strongest radio emission region in SG 13 at 1420 MHz. In addition to the ionized branches present at $l \simeq 111°5'$ and 111°25′, the image at 1420 MHz reveals a weak radio continuum emission at $(l, b) \simeq (111°35', -0°15')$, coincident with a region of diffuse optical emission. Previous high-resolution radio continuum studies of Sh2-157 were centred on SG 14 and did not include the northern SG 13 area (Israel 1977).

The ring nebula around WR 157 can also be identified in the radio continuum surveys at 4850 MHz (Condon et al. 1991) and 2700 MHz (Fürst et al. 1990), taken with the Effelsberg 100-m telescope. These images are not included in this paper.

Clearly, the image at 408 MHz is contaminated with the reduction artefacts from the strong source Cas A, located 2° away from Sh2-157. The sources detected at $(l, b) = (111°10', -0°30')$ and $(l, b) = (111°5', -0°22')$, which are not evident at 1420 MHz, coincide with the X-ray source X 1WGA J23138+6024 and the radio source NVSS J231310+601236, respectively. Both are listed in the NASA/IPAC Extragalactic Database (NED) as extragalactic radio sources. These sources were not included in the flux density estimate.

Derived flux densities (S_ν) at 408, 1420 and 2700 MHz are 1.8 ± 0.9, 3.4 ± 0.9 and 3.5 ± 1.0 Jy, respectively. The uncertainty in flux density arises in both the rms noise of the images and the estimate of the background emission.

Uncertainties in the flux densities are too large to allow a meaningful determination of the spectral index; however, the flux densities are consistent with a thermal origin.

The sources centred at $(l, b) = (111°26', -0°40')$, $(l, b) = (111°18', -0°40')$ and $(l, b) = (111°8', -0°46')$ in the image at 1420 MHz were named as G 111.4-0.7, S 157 A and G 111.2-0.8 by Israel (1977), and correspond to SG 14.

4.2 Infrared emission

The *IRAS* (HIRES) image at 60 μm around the open cluster is displayed in the top panel of Fig. 3. The middle panel displays the MSX band *A* emission centred at 8.28 μm. The 7.6 and 8.6 μm features of the policyclic aromatic hydrocarbons (PAHs) strongly contribute to the emission within this band. The bottom panel of Fig. 3 shows an overlay of the 60 μm (contours) and 8.28 μm (grey-scale) emission distributions.

The emission distribution in the FIR presents the same morphology as in the optical and radio continuum bands. The IR emission at 100 μm, not shown here, displays the same distribution as the 60 μm image. The emission in the FIR originates in the thermal emission from dust. The strong correlation between the FIR and the radio continuum emission suggests that large grains and ionized gas are well mixed.

Strong correlation between the emissions at 60 and 8.28 μm is clear at $(l, b) \simeq (111°12', +0°2')$ and $(l, b) \simeq (111°5', -0°20')$. The 8.28 μm emission distribution coincides with the emission at 60 μm mainly at the right branch at $l \leq 111°20'$. A different behaviour is observed towards $(l, b) = (111°25', -0°15')$, where the bright region at 60 μm coincides with a low-emission region at 8.28 μm. Very probably, the dust grains responsible for the emission at

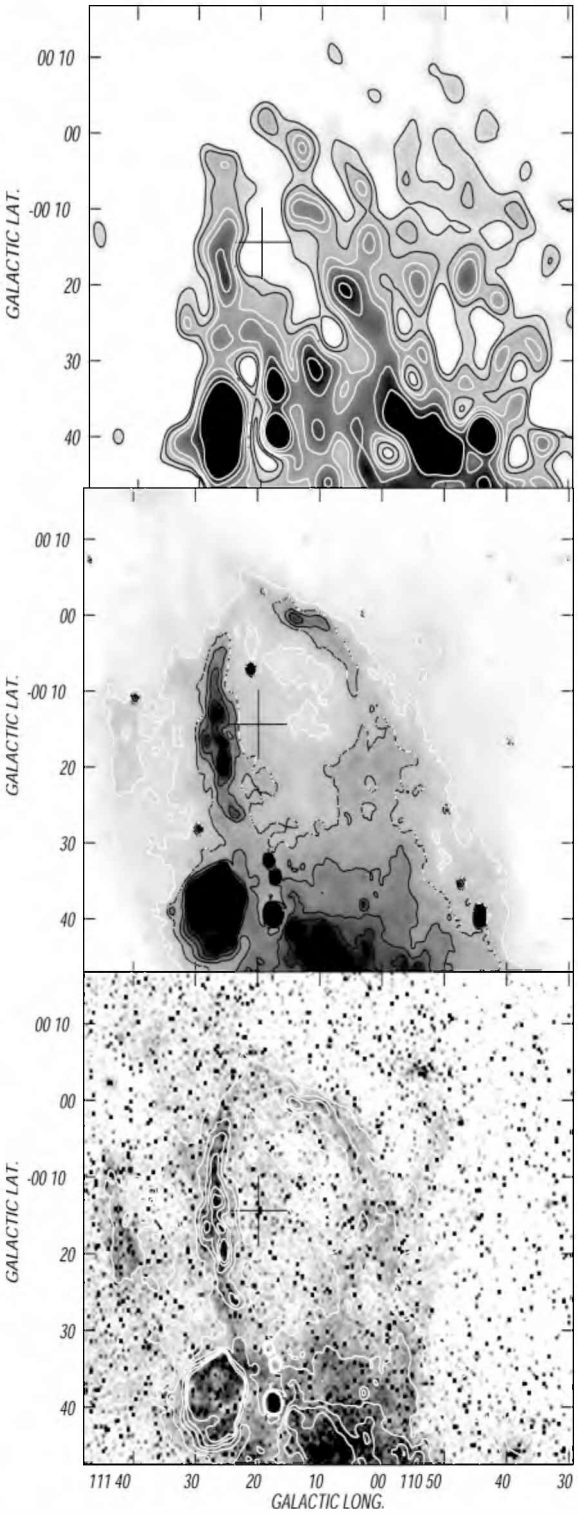

Figure 2. Top panel: radio continuum image at 408 MHz. The grey-scale in brighness temperature T_b corresponds to 110–150 K. The contour lines are 115, 120, 125 130, 140 and 150 K. Middle panel: radio continuum image at 1420 MHz. The grey-scale in T_b corresponds to 7–13 K. The contour lines are 8, 9, 10, 11, 12 and 13 K. The cross marks the position of WR 157. Bottom panel: overlay of the optical emission and the 1420 MHz contour lines.

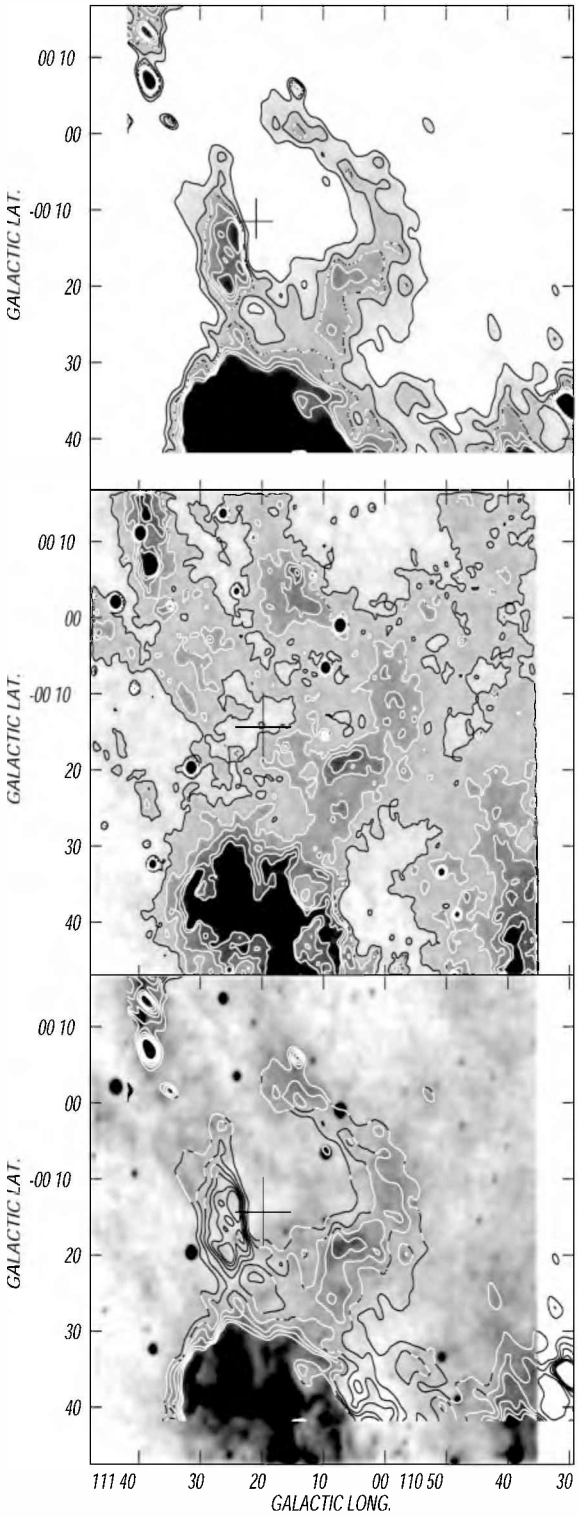

Figure 3. Top panel: *IRAS* image at 60 μm. The grey-scale corresponds to 65–140 MJy sr^{-1}. The contour lines are 70, 80, 90, 100, 110 and 120 MJy sr^{-1}. Middle panel: MSX band *A* at 8.28 μm. The grey-scale is 10.5 (7σ) to 40 MJy sr^{-1} and the contour lines are 16, 21, 26, 31 and 36 MJy sr^{-1}. Bottom panel: overlay of the 60 μm (in contour lines) and the 8.3 μm (grey-scale) emissions.

8.28 μm have been destroyed in this part of the nebula, which is closest to the WR star.

The strongest IR emission region present at $b < -0°30'$ corresponds to SG 14.

4.3 The emission from the molecular gas

The CO(1-0) emission distribution of a larger region is shown in Fig. 4. The left-hand panel shows the result of integrating the emission within the velocity range −58.4 to −43.5 km s^{-1} in grey-scale and contour lines, while the right-hand panel shows an overlay of the contour lines of the left-hand panel and the optical emission. A number of CO cloudlets border the section of the ring nebula towards the lower Galactic longitudes. The brightest optical region, which runs parallel to $l = 111°25'$, appears almost free of molecular material, since only the end-point near $b \simeq -0°5'$ matches a strong CO cloudlet. The CO cloud near $(l, b) = (111°25', -0°32')$ coincides with the low-latitude edge of the ring nebula and separates it from SG 14. Note that the maximun in the CO emission corresponds to an optically faint region. The fragmentary molecular emission delineates a roughly circular structure surrounding the optical ring nebula, as would be expected where an ionized region is surrounded by neutral gas. This is schematically indicated by a dashed circle in the left-hand panel of Fig. 4.

The velocities of the CO gas that surrounds the optical nebula span the interval −55 to −43 km s^{-1}. CO associated with the region at $(l, b) = (111°30', -0°15')$ was detected between −43 and −47 km s^{-1}, while the CO cloud at $(l, b) = (111°25', -0°35')$ is present at $\simeq$ −50 km s^{-1}, and the chain of CO cloudlets spans the velocity interval −55 to −50 km s^{-1}. The region at $(l, b) = (111°35', +0°5')$, apparently unrelated to SG 13, is detected in the velocity range −58 to −48 km s^{-1}. The positional correlation between the optical and CO rim structures and the agreement between the velocities of these cloudlets with the corresponding velocity of the ionized gas (see Section 2) suggest that the molecular feature is the molecular counterpart of SG 13. The clumpy CO morphology suggests that most of the CO gas in the region has been dissociated by the strong UV photon flux of the massive stars in Mrk 50. Considering the whole molecular velocity range, the expansion velocity of the CO ring is 8 ± 1 km s^{-1}.

A large and intense patch of CO emission is present in the northern section of the image. With the exception of the H II region Sh2-159, located at $(l, b) = (111°36', +0°22')$ (Israel 1977), this molecular emission shows little correlation with the optical emission. The strong CO emission projected on to Sh2-159 is very probably associated with the H II region, because of the similar CO and Hα velocities (Blitz et al. 1982).

A comparison of the IR emission distributions at 8.28 and 60 μm (Fig. 3) with the molecular one (Fig. 4) reveals a clear morphological correlation. The CO clouds encircle the IR emission associated with SG 13.

Adopting a systemic CO velocity of −48 km s^{-1} for the molecular gas related to SG 13, the Circular Galactic Rotation model by Brand & Blitz (1993) predicts a kinematical distance $d_{CO} = 5.0 \pm 0.8$ kpc. The uncertainty was derived adopting a velocity dispersion of 6 km s^{-1} for the interstellar gas. The kinematical distance is compatible with the spectrophotometric distance of Mrk 50 and WR 157 (see Section 2).

4.4 The emission of the neutral atomic gas

Fig. 5 exhibits the average H I emission distribution along the line of sight to SG 13. The profile was obtained by averaging the H I

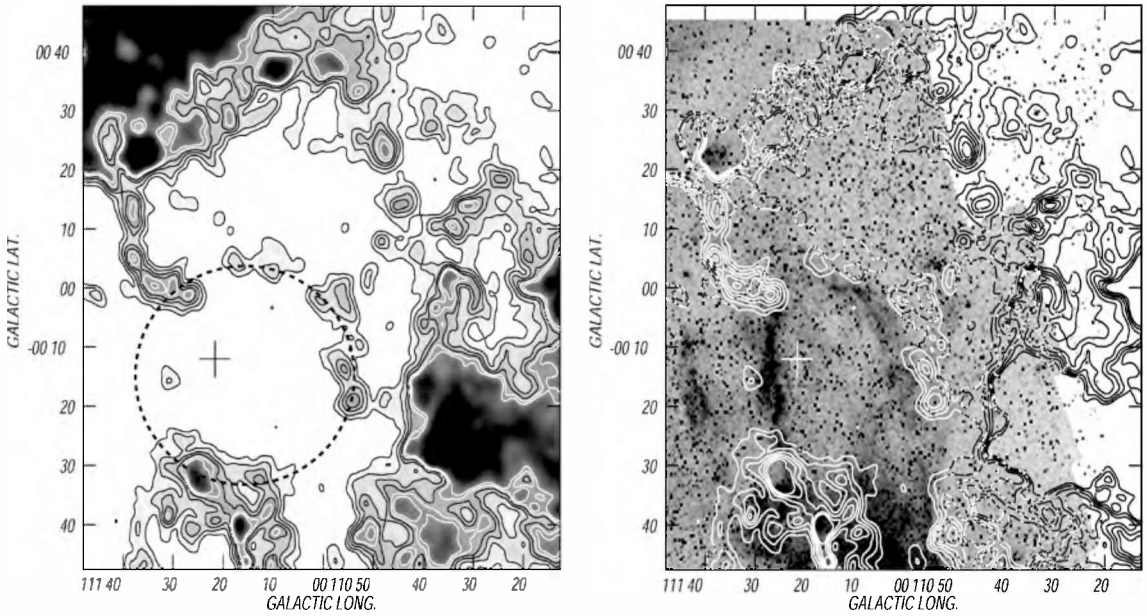

Figure 4. Left-hand panel: integrated CO emission distribution within the velocity range −58.4 to −43.5 km s^{-1}. The grey-scale corresponds to 1.5–50 K km s^{-1}. The contour lines are 2.5, 6, 11, 16, 21 and 26 K km s^{-1}. The dashed circle marks the clumpy CO structure. Right-hand panel: overlay of the DSS *R* image in grey-scale and the CO emission distribution in contour lines.

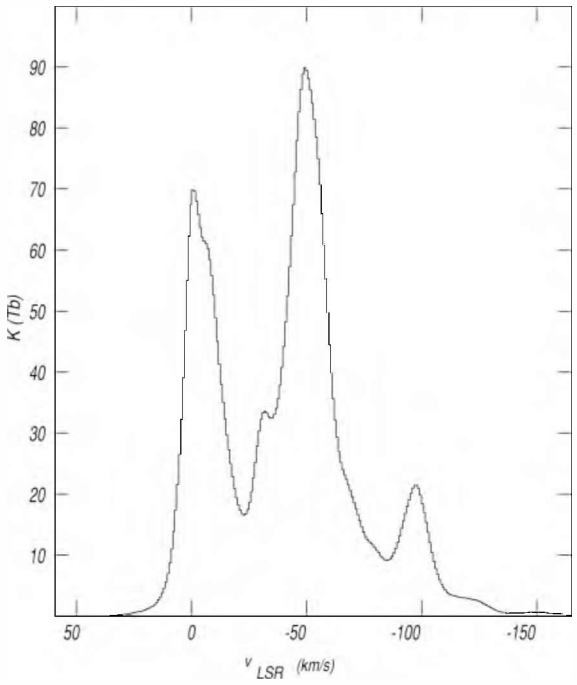

Figure 5. Average H I spectrum towards SG 13.

emission within a box of 1°30′ × 1°45′ enclosing the H II region. The more intense peaks are present at 0 and −50 km s^{-1} with brightness temperature $T_b \sim 70$ and 90 K, respectively, enclosing a central region with a brightness temperature of about ∼20 K. A less-intense peak is centred at ∼ −100 km s^{-1} with $T_b \simeq 20$ K. An analytical fit to the Circular Galactic Rotation model by Brand & Blitz (1993) predicts that the material with velocities of −100 and −50 km s^{-1} should be located at ∼12 and ∼5 kpc, corresponding to the Cygnus and Perseus arms, respectively, while gas at about 0 km s^{-1} corresponds to the Orion arm (local gas).

Fig. 6 displays the superposition of the CO emission distribution shown in Fig. 4 (in contour lines) and the H I brightness temperature T_b distribution within the velocity range −48.0 to −33.2 km s^{-1} in steps of 2.5 km s^{-1}. The analysis of the H I emission distribution within this velocity range allows identification of two structures at velocities compatible with the radial velocities of the ionized and molecular material linked to SG 13. The larger and weaker structure, of about ∼30 arcmin in radius, is centred at $(l, b) = (111°7', +0°8')$ (hereafter Shell A), while the smaller and brighter one, of about 20 arcmin in radius, is centred at $(l, b) = (110°55', -0°35')$ (hereafter Shell B). Both shells are shown in Fig. 6 as white circles.

Shell A is clearly identified at $\simeq$ −44 km s^{-1}. The section of this H I structure at $b \simeq +0°20'$ is associated with the intense CO emission detected at these Galactic latitudes.

Shell B surrounds part of the H II region SG 14. The section of Shell B at $l = 110°47'$ coincides with relatively strong CO emission, while the border at $l = 111°20'$ correlates with faint CO emission linked to SG 14. However, a morphological connection with the IR and radio continuum counterparts of SG 13 is not observed. No CO is detected at the interface between the two H I shells.

The lower right panel of Fig. 7 displays the H I integrated emission in the velocity interval from −44.0 to −41.5 km s^{-1}, corresponding to the systemic velocity of Shell A. The upper and left-hand panels of Fig. 7 show the (v, l) image corresponding to $b = 0°0$ and the (v, b) image for $l = 111°10'$, respectively. These images allow us to estimate the extension in the velocity of Shell A and are useful to derive its expansion velocity. Shell A can be detected within the velocity interval from −32 to −50 km s^{-1}, with an expansion velocity of 13 ± 2 km s^{-1}. Shell B can also be identified in the left-hand panel of Fig. 7, although it is less conspicuous than Shell A. Following Brand & Blitz (1993), we determine a kinematical distance for Shell A of 4.6 ± 0.8 kpc.

The molecular gas related to the section of SG 13 at $(l, b) = (111°10', 0°0')$ appears projected close to the centre of Shell A. The

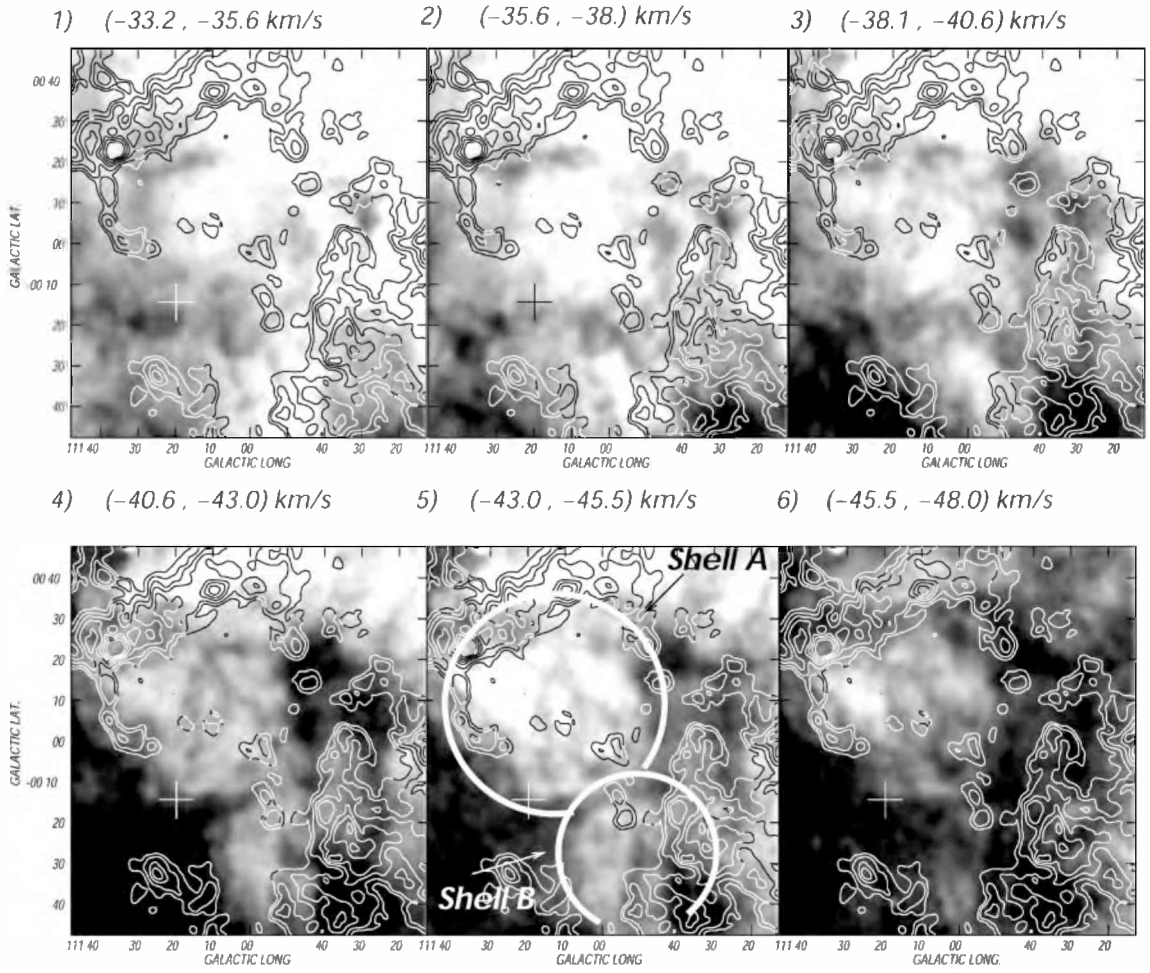

Figure 6. Superposition of the H I emission distribution in the line of sight to Mrk 50 (grey-scale) with the CO integrated emission (contours). Each H I map shows the mean brightness temperature within an interval of ~2.5 km s^{-1}. The grey-scale in T_b of the H I emission is 40–100 K for maps (1), (2), (3) and (4) and 70–135 K for maps (5) and (6). The cross marks the position of WR 157. The white circles delineate Shells A and B detected in H I.

distribution of the molecular material related to SG 13 correlates neither with Shell A nor with Shell B. The analysis of the H I emission distribution spanning the range −48.5 to −51.8 km s^{-1} does not show an obvious H I counterpart to the ionized and molecular gas related to SG 13.

In order to obtain a better view of the general H I environment of the two structures, we present in Fig. 8 a slightly larger field of view than the one used for the previous H I images. The figure is the average of three CGPS channels between −41.86 and −44.34 km s^{-1}, smoothed to a resolution of 2 arcmin. The figure very clearly shows the shell-like structure of feature A.

5 STAR FORMATION

In this section, we consider the possibility that star formation is going on in the expanding shell pushed by the stellar winds of the massive stars in Mrk 50, particularly by WR 157, following the 'collect and collapse' model by Elmegreen & Lada (1977). We look for the presence of young stellar object (YSO) candidates that are projected on to the molecular envelope of SG 13 in the MSX, *IRAS* and Two-Micron All-Sky Survey (2MASS) point-source catalogues. The searched box area was $1^\circ \times 1^\circ$ centred on the position of the open cluster.

We follow the Comerón, Schneider & Russeil (2005) criteria in looking for YSO candidates in the 2MASS point sources catalogue. These criteria discriminate between giant and main-sequence stars with or without reddening and sources with IR excess. The last ones are the most important sources for our purpose since their IR fluxes reveal the presence of circumstellar IR emission. According to these criteria, we found around 20 000 2MASS sources, of which only 19 present IR excess. Fig. 9 displays the colour–magnitude (CM) diagram of the 19 sources with IR excess assuming a distance of 3.7 ± 1.2 kpc. The zero-age main sequence (ZAMS) from O3 to B5 type stars is indicated at the left of the diagram. Half of the IR excess sources present the visual absorption larger than 10 mag. Table 1 summarizes the main parameters of these sources, i.e. galactic coordinates, designation and *J*, *H*, and *K*s magnitudes.

Following the criteria given by Junkes, Fürst & Reich (1992), we have also found that several *IRAS* point sources projected on to this region are protostellar candidates. The data for these sources are compiled in Table 1, which shows the (l, b) coordinates, the *IRAS* name, the fluxes at 12, 25, 60 and 100 μm of each source and the FIR luminosity according to Chan & Fich (1995). We found that nine out of the 17 *IRAS* sources are YSO candidates.

Lumsden et al. (2002) derived several criteria to help identify massive young stellar objets (MYSOs) in the MSX point-source

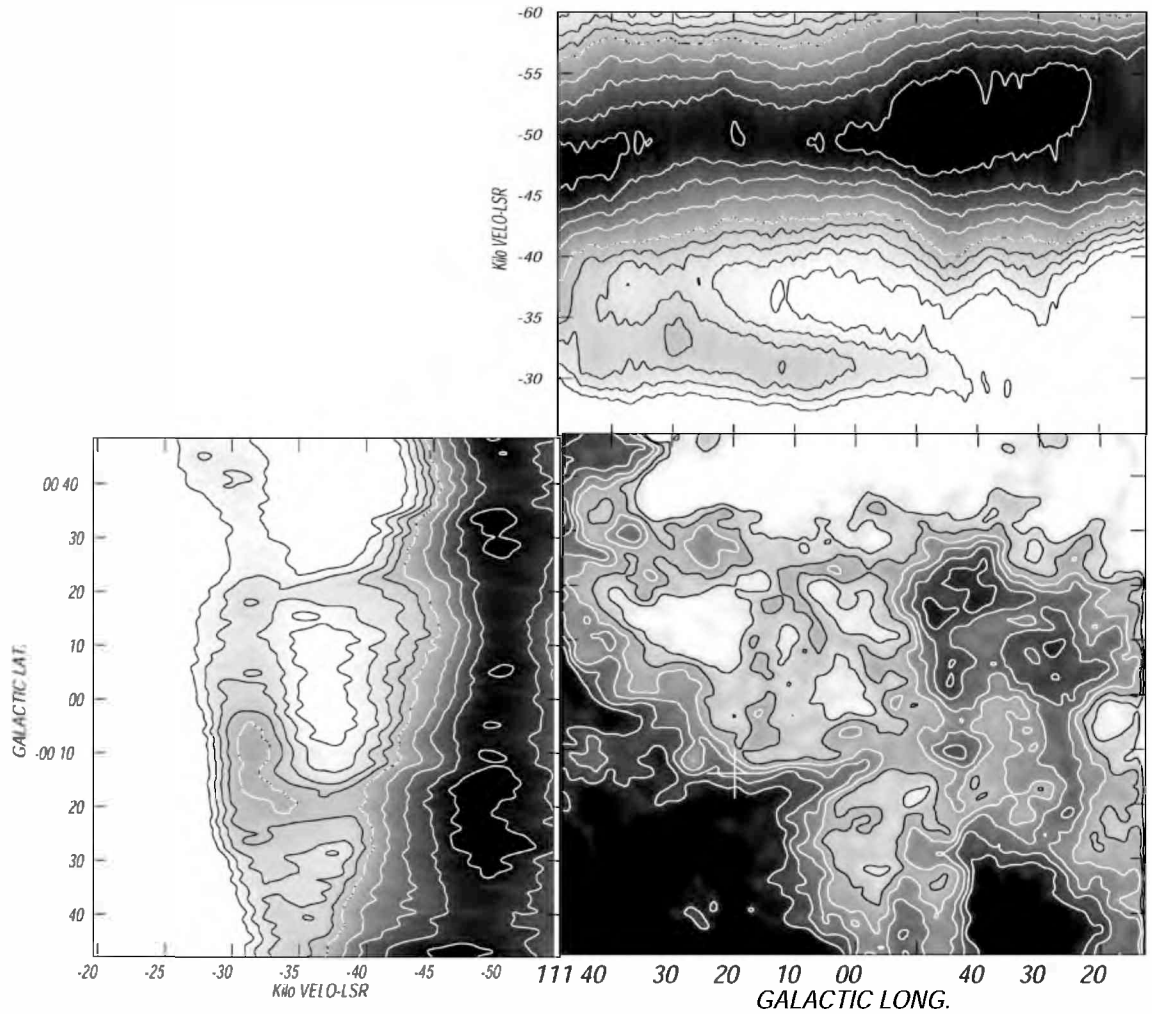

Figure 7. Bottom right panel: H I integrated emission in the velocity interval from −44.0 to −41.5 km s^{-1}, corresponding to the systemic velocity of Shells A and B. The grey-scale is 80–140 K and the contour lines are 70, 80, 90, 100, 110, 120, 130 and 140 K. Upper panel: (v, l) image for $b = 0.^{\circ}0$ showing brightness temperature T_b. Grey-scale: 30–90 K. Contours: 30, 35, 40, 45, 50, 60, 70, 80 and 90 K. Bottom left panel: (v, b) image for $l = 111.^{\circ}9.6$ showing the same grey-scale and contours as the upper panel.

catalogue. The main idea is to discriminate among the sources with IR excess originating in dust envelopes around young and evolved stars, and H II regions. From mid-IR colour–colour diagrams, they found that MYSOs have IR fluxes with ratio $F_{21}/F_8 > 2$ and $F_{14}/F_{12} > 1$, where F_8, F_{12}, F_{14} and F_{21} are the fluxes at 8.28, 12.13, 14.65 and 21.30 μm. For compact H II regions, these flux ratios are $F_{21}/F_8 > 2$ and $F_{14}/F_{12} < 1$. Evolved stars have $F_{21}/F_8 < 2$. On this basis, no YSO candidates are found inside the searching box area.

In Fig. 10, we display the spatial distribution of the YSO candidates of Table 1 projected on to the 1420 MHz image in grey-scale and the ^{12}CO(1-0) emission distribution in contours. The crosses correspond to the objects with IR excess from the 2MASS catalogue and the triangles to *IRAS* protostellar candidates.

IRAS sources 20, 21, 24, and 26 are projected on to CO cloudlets. Sources 25 and 27 appear projected over regions lacking molecular emission, while source 23 coincides with an ionized filament. On the other hand, 2MASS sources 6, 7, 11, 18 and 19 are projected over radio continuum filaments, while sources 2, 5, 12, 13 and 15 coincide with CO clouds. Sources 9, 16 and 17 are projected on to a diffuse ionized region. Sources 1, 4, 8 and 22 are related to the H II region

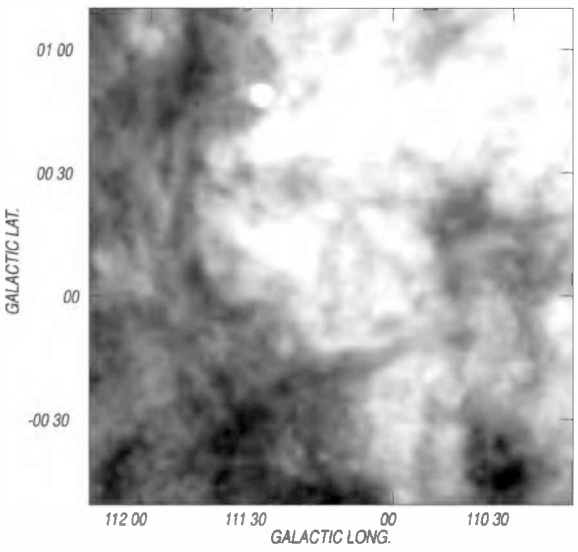

Figure 8. General H I environment around SG 13. The grey-scale is the same as in Fig. 6.

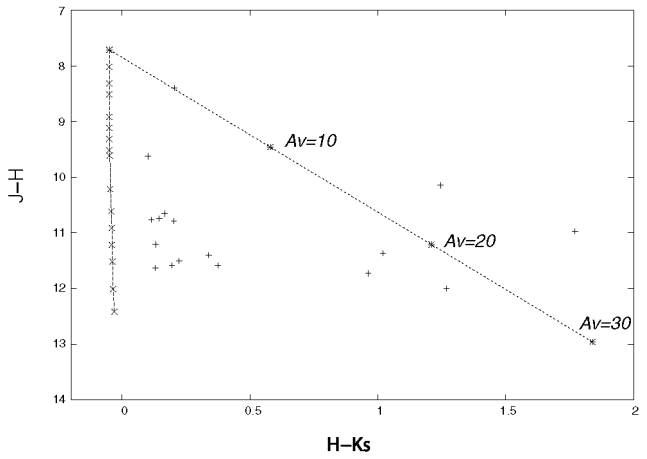

Figure 9. CM diagram of 2MASS point sources with IR excess in direction to SG 13.

SG 14. Finally, sources 14 and 28 are located far away from the molecular emission linked to SG 13.

We conclude that many YSO candidates are projected on to the IB envelope. Besides, we believe that about half of the 2MASS sources having IR excess with $A_v > 10$ mag may evolve towards massive stars. Their strong visual absorption and their location in the CM diagram favour this suggestion. The existence of a relatively large number of 2MASS and *IRAS* YSO candidates reveals the presence of YSO in different evolutionary phases. The spatial distribution of the YSO candidates is suggestive of the action of the 'collect and collapse' process described by Elmegreen & Lada (1977).

6 DISCUSSION

6.1 Main physical parameters of the ring nebula

Table 2 shows the more relevant parameters of the ionized and neutral structures linked to Mrk 50.

The electron density n_e, the ionized mass M_{ion}, the emission measure EM and the observational excitation parameter U_{rad} were determined using the classical expressions by Mezger & Henderson (1967) from the image at 1420 MHz. We assumed that SG 13 is a spherical nebula with constant density. We adopted an electron temperature $T_e = 10^4$ K, and assumed singly ionized He (the derived mass M_{ion} was multiplied by 1.27 to take this fact into account). The estimated rms electron density and the ionized mass, corresponding to a filling factor $f = 1$, are listed in Table 2. Electron densities for $f = 0.1$–0.2 are also included in Table 2. These filling factors were derived by taking into account that SG 13 is a ring of ∼12 arcmin in radius and 5 arcmin in thickness, and that only 10–30 per cent of its surface is covered by plasma.

Based on [S II] emission lines, Lozinskaya et al. (1986) determined the electron densities $n_e' = 100$–150 cm^{-3} for the optical nebula, higher than the values derived from radio continuum

Table 1. YSOs candidates in direction to SG 13.

Number	l(°)	b(°)	2 MASS sources Designation	J (mag)	H (mag)	K_s (mag)		
1	111.41	−0.56	23164713+6010319	15.132	13.265	11.997		
2	111.16	−0.40	23142490+6013421	11.428	11.34	11.209		
3	111.19	−0.24	23141131+6023109	8.756	8.603	8.399		
4	111.29	−0.68	23161127+6001148	14.002	12.06	10.642		
5	110.91	−0.22	23120304+6018385	13.062	11.392	10.147		
6	111.08	−0.30	23133130+6017273	13.473	12.383	11.363		
7	111.06	−0.27	23131651+6019056	11.844	11.76	11.63		
8	111.41	−0.53	23164107+6011498	13.713	12.691	11.729		
9	111.61	−0.33	23173713+6027406	9.727	9.727	9.626		
10	111.34	−0.10	23145423+603425	12.391	11.956	11.582		
11	111.07	−0.12	23125722+6027223	11.979	11.728	11.505		
12	111.06	0.097	23121250+6039495	10.977	10.884	10.739		
13	111.18	−0.10	23134236+6031201	11.932	11.779	11.584		
14	111.72	0.03	23172558+6050436	7.461	5.98	4.826		
15	111.64	0.04	23164590+6049490	15.606	12.742	10.971		
16	111.56	−0.16	23164539+6035553	10.929	10.82	10.654		
17	111.37	0.04	23144274+6043428	11.194	10.99	10.788		
18	110.99	−0.51	23132696+6003570	10.932	10.883	10.769		
19	110.90	−0.41	23122993+6007256	12.191	11.742	11.404		
			IRAS sources					
				Fluxes				L_{FIR}
				12 μm (Jy)	25 μm (Jy)	60 μm (Jy)	100 μm (Jy)	(Jy)
20	110.88	0.01	23088+6014	0.38	0.41	6.38	28.79	157.92
21	111.23	0.10	23113+6027	0.54	0.83	8.64	40.40	220.55
22	111.42	−0.56	23146+5954	7.17	15.0	275.0	671.0	4324.25
23	111.45	−0.31	23141+6008	0.46	0.21	8.22	38.79	210.13
24	111.58	0.02	23141+6030	0.71	1.05	9.60	44.90	245.51
25	111.58	−0.12	23146+6022	0.81	0.97	5.88	32.70	174.00
26	111.63	0.11	23143+6036	0.93	1.30	28.39	116.0	648.31
27	111.66	−0.08	23151+6026	0.95	0.52	4.40	23.0	123.88
28	111.73	0.03	23152+6034	22.20	25.10	147.0	227.0	1800.00

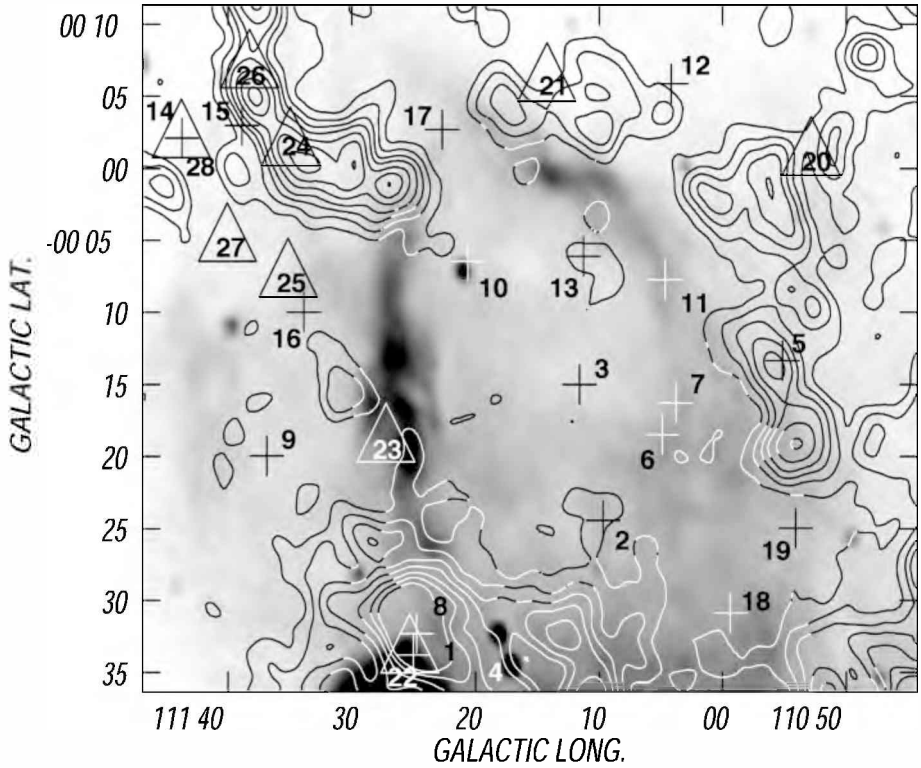

Figure 10. Spatial distribution of YSO cantidates in direction to SG 13 over the image at 1420 MHz in grey-scale from 7 to 13 K, and the ^{12}CO image with the following contours: 1.5, 5, 10, 20, 30 and 40 K km s^{-1}. The 2MASS and *IRAS* sources are indicated by crosses and triangles, respectively.

observations. Following Israel (1978), a different estimate for the filling factor can be obtained as $f = (ne/ne')^{0.5} = (2\text{–}7) \times 10^{-3}$. Electron densities derived from optical line ratios are higher than the ones obtained from radio continuum observations. The former corresponds to the regions with high emissivity and high electron densities, while the latter have a large contribution from the low electron density regions. Very probably, the real f is in between these two values.

$U_{\rm rad}$ is related to the number of UV photons used to ionize the gas and is obtained as $U_{\rm rad} = Rn_{\rm e}^{2/3}$, where R is the radius of the ionized gas. U_* is linked to the number of UV photons emitted by the massive stars in the open cluster, which can be obtained from atmosphere models. To estimate U_*, we took into account only WR 157 (WN5 star), since the other stars in Mrk 50 have spectral types later than B3 (Baume et al. 2004). Following Smith, Norris & Crowther (2002), $U_* \simeq 128$ pc cm^{-2}. From Table 2, $U_{\rm rad} < U_*$, indicating that the UV photons emitted by the WR star are enough to ionize the gas. A large number of UV photons probably escape to the ISM through the clumpy molecular envelope around SG 13 and/or are absorbed by the associated dust, warming and destroying it.

Bearing in mind that the interstellar dust radiates in the FIR, we derived the dust mass $M_{\rm d}$ associated with SG 13 and the dust colour temperature $T_{\rm d}$ from the emission at 60 and 100 μm (Draine & Lee 1984). The absorption coefficient χ_ν of the dust can be written as

$$\chi_\nu = 4 \left(\frac{\nu}{3 \times 10^{12}\,{\rm Hz}} \right)^n \ {\rm kg^{-1}\,m^2}, \tag{1}$$

where $n = 1\text{–}1.5$ is the dust spectral index. $T_{\rm d}$ can be obtained as

$$T_{\rm d}(K) = \frac{95.94}{\ln\left[(1.67)^{3+n}\,(S_{100}/S_{60})\right]}. \tag{2}$$

S_{100} and S_{60} are the IR fluxes at 100 and 60 μm. For $n = 1\text{–}1.5$, $T_{\rm d} \simeq 28\text{–}31$ K. Following Hildebrand (1983), the dust mass is

$$M_{{\rm d},\nu} = \frac{S_\nu d^2}{\chi_\nu B_\nu(T_{\rm d})}, \tag{3}$$

where $B_\nu(T_{\rm d})$ is the blackbody function. The flux densities at 60 and 100 μm, along with the derived dust mass, are listed in Table 2.

The associated molecular mass of each cloudlet, $M_{\rm H_2}$, can be obtained as

$$M_{\rm H_2} = \mu\, m_{\rm H}\, d^2\, \Omega\, N_{\rm H_2}. \tag{4}$$

We adopted $\mu = 2.76$ for the molecular weight (assuming solar abundances), $m_{\rm H}$ is the atomic hydrogen mass, Ω is the solid angle of the molecular cloudlet and $N_{\rm H_2}$ is the H_2 column density, which is obtained as

$$N_{\rm H_2} = X\, I_{\rm CO}, \tag{5}$$

where $X = 1.9 \times 10^{20} \frac{\rm mol\,cm^{-2}}{\rm K\,km\,s^{-1}}$ (Grenier & Lebrum 1990; Digel, Hunter & Mukherjee 2002). $I_{\rm CO}$ is the integrated emission of the CO line. The mean column density and the molecular mass are listed in Table 2.

The gas-to-dust ratio derived taking into account the ionized and molecular masses listed in Table 2 is ~20, lower than the typical value of ~100 generally accepted for H II regions.

6.2 Origin and scenario

Assuming the CO expansion velocity of 8 ± 1 km s^{-1} listed in Table 2, the dynamical age of SG 13, according to wind bubble evolutionary models, is $t_{\rm d} = 0.55\, R_{\rm mol}/v_{\rm exp} = (1.4 \pm 0.4) \times 10^6$ yr. Considering the radio continuum, IR and molecular counterpart

Table 2. Physical parameters of SG 13's counterparts.

Distance adopted	3.7 ± 1.2 kpc
Radio continuum	
S_{2700} (Jy)	3.5 ± 1.0
S_{1420} (Jy)	3.4 ± 0.9
S_{408} (Jy)	1.8 ± 0.9
Spectral index, α	
408 and 1420 MHz	$+0.5 \pm 0.3$
1420 and 2700 MHz	$+0.03 \pm 0.1$
Angular radius (arcmin)	12 ± 3
Linear radius R (pc)	15 ± 4
$n_e(f = 1)$	4 ± 1
$M_{ion}(f = 1)(M_\odot)$	3700 ± 600
$n_e(f = 0.1$–$0.2)(cm^{-3})$	15-9
$M_{ion}(f = 0.1$–$0.2)(M_\odot)$	1100–1500
U_{rad} (pc cm^{-2})	45
U_* (pc cm^{-2})	~ 128
EM (pc cm^{-6})	$(2.4 \pm 1.7) \times 10^3$
IR	
S_{60} (Jy)	$\sim 6.9 \times 10^3$
S_{100} (Jy)	$\sim 2.25 \times 10^4$
Dust colour temperature (K)	28–31
Dust mass ($M_\odot$)	90 ± 55
^{12}CO	(1-0)
(l, b) centroid of IB	$111°5', -0°4'$
Velocity range Δv(km s^{-1})	-58.4 to -43.5
Expansion velocity (km s^{-1})	8 ± 1
Angular radius of the shell R_{mol} (arcmin)	17.5 ± 3.0
Linear radius of the shell (pc)	18 ± 5
H^2 mean column density (cm^{-2})	$(2.9 \pm 1.3) \times 10^{20}$
H^2 mass of the shell ($M_\odot$)	$(8.2 \pm 1.7) \times 10^2$

of SG 13, the kinematic energy of the IB is $E_k = (9.8 \pm 6.0) \times 10^{47}$ erg.

Assuming typical values for the stellar wind of a WN 5 star, a mass-loss rate $\dot{M} = 1.75 \times 10^{-5}\,M_\odot\,yr^{-1}$ and a terminal velocity $v_\infty = 1520$ km s^{-1} (Smith et al. 2002; Cappa et al. 2004), and assuming a previous O-type phase with values of $\dot{M} = 2.3 \times 10^{-7}\,M_\odot\,yr^{-1}$ and $v_\infty = 1950$ km s^{-1} (Smith et al. 2002), we obtain a mechanical luminosity for the stellar wind of WR 157 during the O and WR phases, $L_O \simeq 3.5 \times 10^{35}$ erg s^{-1} and $L_W \simeq 1.3 \times 10^{37}$ erg s^{-1}, respectively. Bearing in mind a lifetime $t_O = 5 \times 10^6$ yr for the O-type phase of a star with an initial mass of $40\,M_\odot$ and $t_{WR} = 0.4 \times 10^6$ yr for the WR phase (Meynet et al. 1994), the mechanical energy injected into the ISM in each evolutionary phase is $E_{w_O} \simeq 5.5 \times 10^{49}$ erg and $E_{w_{WR}} \simeq 1.6 \times 10^{50}$ erg.

The ratio $\epsilon = E_k/E_w$ estimated considering only the WR phase of WR 157 is 6×10^{-3}. We can conclude that the stellar wind of the WR star alone is the main one responsible for shaping the IB around the open cluster.

The distributions of the interstellar dust and the ionized and molecular material in the environs of Mrk 50 can be explained as the consequence of the action of the stellar winds of WR 157. As regard H I gas, no neutral atomic counterpart of SG 13 could be identified from the present study, since the spatial distribution of Shells A and B is very different from that of SG 13. It is likely that the small amount of H I gas resulting from the photodissociation of the molecular gas would be hardly detectable against the strong background H I emission.

As regards the ionized gas, we can suggest two possible scenarios.

(i) The inner bright optical filaments were probably generated by the action of the present WR phase of the star. The shock fronts have ionized and dissociated the molecular circumstellar environment creating photodissociated regions. The outer optical filaments may have been swept- up by the stellar winds in earlier stellar phases.

(ii) The other possibility is that the distribution of the different optical filaments is far from being coplanar. If this were the case, we would be observing the projection of the filaments over the plane of the sky, the real dimensions of the structures being then larger than indicated in Table 2.

7 CONCLUSION

Using the CGPS high-resolution radio continuum and 21-cm H I line data, supplemented by previous optical, IR and CO surveys, we arrive at the following conclusions concerning the ring nebula SG13 and the associated star WR 157.

The radio continuum emission correlates extremely well with the optical DSS R and IR 60-μm images. Interference effects from nearby Cas A limit our ability to reliably determine the spectral index between the two CGPS radio frequencies; however, the spectral index between 1420 MHz (CGPS) and 2700 MHz (Fürst et al. 1990) is consistent with thermal emission.

A partial ring of CO emission in the range -56 to -43 km s^{-1} is seen to circumscribe the optical, IR (60 μm) and radio continuum emission of SG13. This range of velocities is consistent with previously measured velocity determinations by Lozinskaya et al. (1986) and Pedlar (1980), based on the optical lines and the H166 radio recombination line, respectively.

An analysis of the spatial distribution of IR point sources having colours characteristic of YSOs shows that an excess of such sources appears projected over the molecular ring surrounding SG13, suggesting thatthe star formation triggered by the stellar members of Mrk 50, in particular WR 157, is taking place.

The kinematics and dynamics of the gas, dust and molecular material around SG13 are entirely compatible with the hypothesis that the WR star alone is responsible for shaping the ISM around the open cluster Mrk 50.

A 50-arcmin diameter H I shell (shell A) is detected in the -32 to -50 km s^{-1} range to the north of SG13. Although this range partially overlaps the velocity range of the CO ring surrounding SG13, this H I structure is entirely distinct from the other structures (molecular ring, optical, IR and radio continuum). The star WR 157 appears projected on to the southern boundary of this H I shell. An expansion velocity of 13 ± 2 km s^{-1} is inferred from a velocity–position diagram. A second, smaller, H I cavity (shell B) is also detected in the velocity range -52 to -41 km s^{-1}, suggesting a lower expansion velocity of 9 ± 2 km s^{-1}. It too does not coincide with any of the structures associated with SG13. We conclude that these two cavities or shells are unlikely to be physically related to SG13.

The lack of an H I shell, which has been detected associated with a large member of IBs, is probably due to a low column density of the H I gas resulting from the photodissociation of the molecular gas.

ACKNOWLEDGMENTS

We acknowledge the referee, Dr Peter Phillips, for his useful suggestions and comments. This project was partially financed by the Consejo Nacional de Investigaciones Científicas y Técnicas (CONICET) of Argentina under project PIP 5886/05, Universidad Nacional de La Plata (UNLP) under project 11/G072 and Agencia Nacional de Promoción Científica y Tecnológica (ANPCYT) under

project PICT 14018/03. The DSS was produced at the Space Telescope Science Institute under US Government grant NAGW-2166. This work was partly (SP) supported by the Natural Sciences and Engineering Research Council of Canada (NSERC) and the Fonds FQRNT of Québec. The DRAO Synthesis Telescope is operated as a national facility by the National Research Council of Canada. The CGPS is a Canadian project with international partners and is supported by the grants from NSERC. Data from the CGPS are publicly available through the facilities of the Canadian Astronomy Data Centre (http://cadc.hia.nrc.ca) operated by the Herzberg Institute of Astrophysics, NRC.

REFERENCES

Baume G., Vazquez R. A., Carraro G., 2004, MNRAS, 355, 475
Blitz L., Fich M., Stark A. A., 1982, ApJS, 49, 183
Brand J., Blitz L., 1993, A&A, 275, 67
Cappa C. E., Rubio M., Goss W. M., 2001, AJ, 121, 2664
Cappa C., Goss W. M., Pineault S., 2002, AJ, 123, 3348
Chan G., Fich M., 1995, AJ, 109, 2611
Comerón F., Schneider N., Russeil D., 2005, A&A, 433, 955
Condon J. J., Broderick J. J., Seielstad G. A., 1991, AJ, 102, 2041
Conti P. S., 1976, Mem. Soc. R. Sci. Liege, 9, 193
Digel S. W., Hunter S. D., Mukherjee, 1995, ApJ, 441, 270
Draine B. T., Lee H. M., 1984, ApJ, 285, 89
Egan M. P., Price S. D., Moshir M. M., Cohen M., Tedesco E., 1999, STIN, 0014854
Elmegreen B. G., 2000, ApJ, 530, 277
Elmegreen B. G., Lada C. J., 1977, ApJ, 214, 725
Fürst E., Reich W., Reich P., Reif K., 1990, A&AS, 85, 61
Georgelin Y. M., Georgelin Y. P., 1976, A&A, 49, 57
Georgelin Y. M., Georgelin Y. P., Roux S., 1973, A&A, 25, 337
Grenier I. A., Lebrum F., 1990, ApJ, 360, 129
Hildebrand R. H., 1983, QJRAS, 24, 267
Israel F. P., 1977, A&A, 59, 27
Israel F. P., 1978, A&A, 70, 769
Junkes N., Fürst E., Reich W., 1992, A&AS, 261, 289
Landecker T. L. et al., 2000, A&AS, 145, 509
Leitherer C., Chapman J. M., Koribalski B., 1997, ApJ, 481, 898
Lozinskaya T. A., Sitnik T. G., Lomovskii A. I., 1986, Ap&SS, 121, 357
Lumsden S. L., Hoare M. G., Oudmaijer R. D., Richards D., 2002, MNRAS, 336, 621
Lündstron I., Stenholm B., 1984, A&AS, 58, 163
McClure-Griffiths N. M., Dickey J. M., Gaensler B. M., Green A. J., Haverkorn M., Strasser S., 2005, ApJS, 158, 178
Maeder A., 1983, A&A, 120, 113
Meynet G., Maeder A., Schaller G., Schaerer D., Charbonnel C., 1994, A&AS, 103, 97
Mezger P. G., Henderson A. P., 1967, ApJ, 147, 471
Oey M. S., 1996, PASP, 108, 5470
Pedlar A., 1980, MNRAS, 192, 179
Ridge N. A. et al., 2006, AJ, 131, 2921
Shain C. A., 1951, AuSRA, 4, 258
Sharpless S., 1959, ApJS, 4, 257
Smith L. J., Willis A. J., 1994, Ap&SS, 221, 189
Smith L. J., Norris R., Crowther P. A., 2002, MNRAS, 337, 1309
Taylor A. R. et al., 2003, AJ, 125, 3145
Turner D. G., Moffat A. F. J., Lamontagne R., Maitzen H. M., 1983, AJ, 88, 1199
van der Hucht K., 2001, New Astron. Rev., 45, 135
Vasquez J., Cappa C., McClure-Griffiths N. M., 2005, MNRAS, 362, 681

This paper has been typeset from a TEX/LATEX file prepared by the author.